JOURNAL OF NANO- AND ELECTRONIC PHYSICS
Vol. **18** No 4, 04008(8pp) (2026)

ЖУРНАЛ НАНО- ТА ЕЛЕКТРОННОЇ ФІЗИКИ
Том **18** № 4, 04008(8cc) (2026)

OPEN ACCESS

REGULAR ARTICLE

Moire-Angle-Controlled Electronic Transport in MoS_2/WS_2 Van der Waals Nanodevices with Graphene and Silicene Electrodes

D. Sergeyev[1,2,*], E. Yeskibayev[2]

[1] *K. Zhubanov Aktobe Regional University, 030000 Aktobe, Kazakhstan*
[2] *T. Begeldinov Aktobe Avation Institute, 030012 Aktobe, Kazakhstan*

(Received 25 March 2026; revised manuscript received 18 August 2026; published online 21 August 2026)

We present a theoretical investigation of electronic transport in van der Waals nanodevices based on MoS_2/WS_2 heterobilayers with various electrode configurations, including graphene- and silicene-based contacts. The influence of relative twisting between the MoS_2 and WS_2 layers is systematically analyzed for twist angles $\theta = 0°$, 3°, 6.2°, and 9.7°, corresponding to different regimes of moiré superlattice modulation. Quantum transport calculations are performed within the nonequilibrium Green's function formalism, enabling a consistent description of contact effects and voltage-dependent transmission characteristics. It is shown that in the absence of twisting, the transport properties are predominantly governed by the electrode material. The introduction of a small twist angle leads to current suppression due to localization of electronic states induced by the moiré effect, whereas larger twist angles result in enhanced conductance. The inverted silicene–MoS_2/WS_2–graphene configuration exhibits the highest current, which is attributed to interface metallization arising from the silicene-MoS_2 contact. These results demonstrate that both the twist angle and the electrode material provide efficient means for tuning the transport properties of MoS_2/WS_2-based nanoelectronic devices.

Keywords: MoS_2/WS_2 Van der Waals nanodevices, TMD Moiré heterostructures, Quantum transport, Contact-induced effects, Nonequilibrium Green's function.

DOI: 10.21272/jnep.18(4).04008 PACS numbers: 07.05.Tp, 73.63. – b

1. INTRODUCTION

Van der Waals (vdW) heterostructures based on two-dimensional materials have emerged in recent years as one of the key platforms for exploring novel quantum and electronic phenomena in nanoelectronics [1-3]. The ability to assemble materials layer by layer with distinct electronic characteristics, without stringent requirements on lattice matching, has enabled the development of functional devices with tunable transport and spectral properties [4, 5]. Of particular interest are heterostructures in which a relative rotational misalignment between the layers leads to the formation of a moiré superlattice, resulting in a substantial modification of the electronic structure of the system [6, 7].

Moiré effects in two-dimensional materials manifest as a spatially periodic potential with a characteristic length scale that is significantly larger than the lattice constant of the constituent crystals [8-10]. Such a superlattice gives rise to the formation of minibands, pseudogaps, localized states, and pronounced modifications of the electronic density of states near the Fermi level. The most prominent example is twisted bilayer graphene, in which correlated insulating and superconducting phases emerge at the so-called "magic" angle [11]. However, in contrast to graphene-graphene systems, heterostructures based on transition metal dichalcogenides (TMDs), such as MoS_2 and WS_2, exhibit a richer variety of physical phenomena due to the presence of a direct band gap, strong spin-orbit coupling, and pronounced sensitivity to external fields and contact effects.

MoS_2/WS_2 heterobilayers constitute a promising class of vdW systems in which differences in band gap, carrier effective masses, and spin-orbit splitting is inherently combined [12-14]. Relative rotational misalignment between the MoS_2 and WS_2 layers gives rise to a moiré modulation that can substantially reconstruct the band structure and induce localized states within the potential minima of the superlattice. These effects have a direct impact on electrical transport, particularly in vertical or planar device geometries, where the current is governed by quantum tunneling and interlayer scattering.

Electrodes play an equally important role in shaping the electrical transport characteristics of such systems [15, 16]. Graphene, owing to its linear energy dispersion, high carrier mobility, and quasi-symmetric coupling to TMD layers, is often employed as a reference electrode. At the same time, silicene – a two-dimensional analogue of silicon with pronounced spin–orbit coupling and strong sensitivity to the substrate and external electric fields – offers additional opportunities for transport control and the realization of asymmetric contact configurations. The use of various combinations of graphene and silicene electrodes enables a systematic investigation of the influence of con-

* Correspondence e-mail: serdau82@gmail.com

Cite this article as: D. Sergeyev, et al., *J. Nano- Electron. Phys.* 18 No 4, 04008 (2026) https://doi.org/10.21272/jnep.18(4).04008

tact effects, work function alignment, and density of states on the *I-V* characteristics of the devices.

In this work, we investigate the electrical transport properties of vdW heterostructures of three types: graphene-MoS_2/WS_2-graphene, graphene-MoS_2/WS_2-silicene, and silicene-MoS_2/WS_2-graphene. Particular attention is paid to the effect of the moiré twist angle between the MoS_2 and WS_2 layers, chosen as 3°, 6.2°, and 9.7°, which correspond to different regimes of the moiré periodicity length – from long-period superlattices with pronounced localization to short-period modulations approaching an effective averaged potential. This selection of twist angles enables a systematic analysis of the evolution of transport characteristics as a function of the moiré length scale.

To analyze electrical transport, we employ the quantum-mechanical nonequilibrium Green's function (NEGF) formalism, which enables a consistent treatment of contact effects, applied bias voltage, and the energy-dependent transmission of the device. *I-V* characteristics and differential conductance are calculated, directly reflecting features of the moiré electronic structure such as miniband edges and pseudogaps. A comparison between symmetric and asymmetric contact configurations allows the role of electrodes in shaping transport nonlinearity and rectifying behavior to be elucidated.

Thus, the aim of this work is to provide a comprehensive investigation of the combined effects of the moiré twist angle and electrode type on the electrical transport characteristics of MoS_2/WS_2 heterostructures. The obtained results are important both for the fundamental understanding of quantum transport in moiré systems and for the development of advanced nanoelectronic devices based on two-dimensional materials, including logic elements, rectifiers, and sensor structures with tunable properties.

2. DEVICE GEOMETRY AND MODEL

The vdW nanodevices considered in this work are multilayer heterostructures formed from two-dimensional materials with atomically thin layers and weak interlayer coupling. Three types of devices are investigated: graphene-MoS_2/WS_2-graphene, graphene-MoS_2/WS_2-silicene, and silicene-MoS_2/WS_2-graphene, which differ in the materials of the left and right electrodes while sharing an identical central active region (Fig. 1).

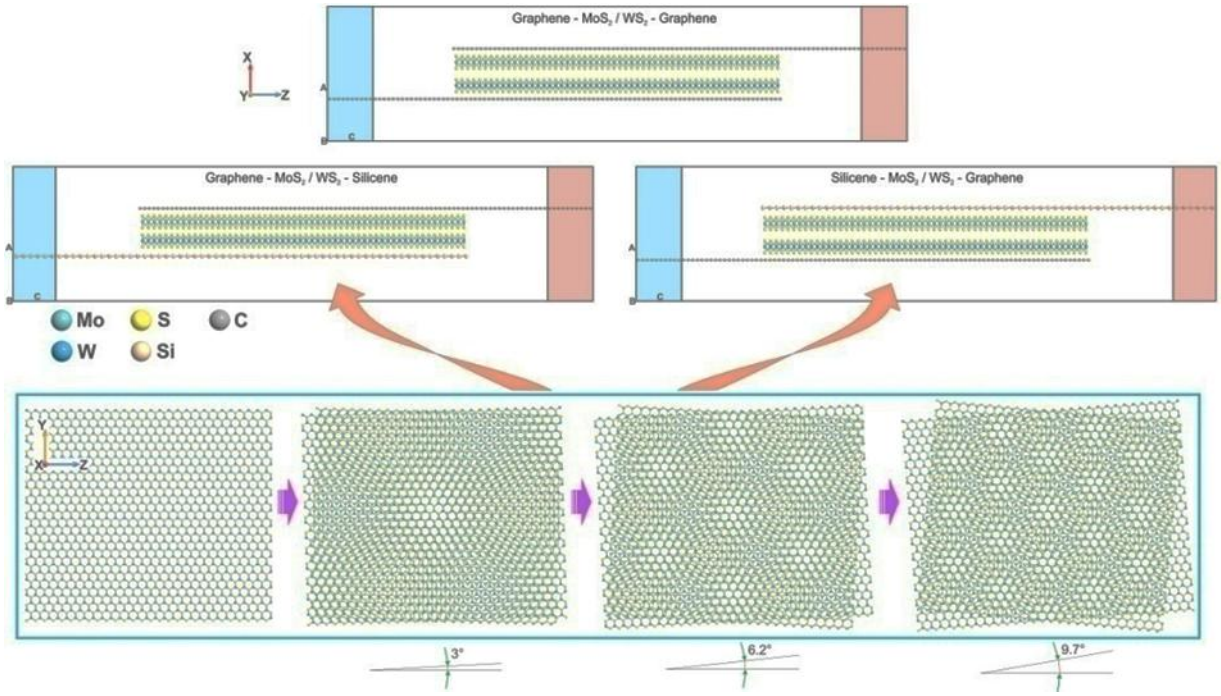

Fig. 1 – Schematic geometry of MoS_2/WS_2 van der Waals nanodevices with graphene and silicene electrodes and different moiré twist angles

The central part of the nanodevice consists of a MoS_2/WS_2 heterobilayer, in which the MoS_2 and WS_2 planes are oriented parallel to each other and separated by an interlayer distance of approximately 3.54 Å, characteristic of vdW heterostructures based on transition metal dichalcogenides. The relative rotation between the MoS_2 and WS_2 layers is defined by a moiré twist angle $\theta = 3°$, 6.2°, and 9.7°, leading to the formation of a moiré superlattice with different spatial periods. The choice of these angles enables the investigation of the transition from long-period moiré modulation to a shorter-period regime approaching an effective averaged potential.

The MoS_2/WS_2 core of the nanodevice has a rectangular geometry with in-plane dimensions of 87.2 Å × 74.82 Å. This region forms the active transport channel, where quantum tunneling of charge carriers and the formation of moiré-induced electronic states take place. The total length of the central device region along the transport direction (the z axis), excluding the electrodes, is 131.526 Å, which is sufficient to establish a steady-state nonequilibrium transport regime.

The electrodes are modeled as semi-infinite two-dimensional graphene or silicene layers oriented per-

pendicular to the transport direction. The length of each graphene electrode within the simulation cell is 12.305 Å, which is adequate for a proper description of the contact regions and their coupling to the central device within the NEGF formalism. The interlayer distance between graphene and the MoS_2 and WS_2 layers is set to approximately 2.169 Å, consistent with typical vdW gaps for graphene-TMD contacts and ensuring a realistic description of interlayer tunneling. The interlayer distance between silicene and the MoS_2 and WS_2 layers is approximately 2.44 Å.

All layers are assumed to be ideal, free of structural defects and vacancies, and the electrode edges are treated as periodic in the direction perpendicular to the current flow. A Cartesian coordinate system is employed, in which the transport direction coincides with the *z* axis, while the planes of the two-dimensional layers lie in the *x-y* plane. This geometrical configuration allows the spatial moiré modulation to be directly correlated with features of electronic transport, including nonlinearity in the I-V characteristics and the emergence of characteristic peaks in the differential conductance.

The described geometry serves as a baseline model for subsequent quantum transport analysis and enables a systematic investigation of the effects of the moiré twist angle, interlayer distances, and electrode material on the electrical transport properties of MoS_2/WS_2 vdW heterostructures.

3. METHODS

Computational modeling of the transport characteristics of two-dimensional heterostructures was carried out within the framework of density functional theory (DFT) combined with the non-equilibrium Green's function (NEGF) formalism, employing the generalized gradient approximation in the Perdew-Burke-Ernzerhof (GGA-PBE) parametrization [17, 18]. To obtain the *I-V* characteristics and the differential conductance, the transmission spectrum of the nanodevice was first calculated as follows:

$$T(\varepsilon) = \mathrm{tr}\left[\Gamma^L G \Gamma^R G^\dagger\right] = \mathrm{tr}\left[\Gamma^R G \Gamma^L G^\dagger\right] \quad (1)$$

where $\Gamma^{L(R)}(\varepsilon)$ is the broadening matrices (broadening functions) of the left (right) electrodes, $G(\varepsilon)$, $G^\dagger(\varepsilon)$ are the retarded and advanced Green's functions.

The *I-V* characteristics of the nanostructure were subsequently calculated using the well-known Landauer formula, which establishes the fundamental relationship between the electrical current and the transmission spectrum:

$$I(V_L, V_R, T_L, T_R) = \frac{2e}{h} \times \int_{-\infty}^{+\infty} T(E)\left[f\left(\frac{E-\mu_R}{k_B T_R}\right) - f\left(\frac{E-\mu_L}{k_B T_L}\right)\right] dE \quad (2)$$

where k_B is the Boltzmann constant, T_L, T_R are the Fermi-Dirac distribution functions, μ_R, μ_L are the electrochemical potentials of the left and right electrodes, respectively.

The differential conductance of the nanostructure was obtained by calculating the self-consistent current for a series of applied bias voltages, followed by numerical differentiation:

$$\sigma(V_{bias}, T_L, T_R) = \frac{I(V^1_{bias}, T_L, T_R) - I(V^2_{bias}, T_L, T_R)}{V^1_{bias} - V^2_{bias}} \quad (3)$$

The electronic transport calculations were performed using a Poisson solver and Brillouin zone integration with a *k*-point sampling grid of (1, 1, 100). A cutoff energy of 75 Hartree was used for the real-space grid, and the convergence criteria for both forces and total energy were set to 10^{-6}.

All simulations were carried out on a Supermicro server equipped with an Intel® Xeon® Silver processor, 512 GB of RAM, and 64 CPU cores. The transport properties of the nanoheterostructures were modeled using the Atomistix ToolKit with Virtual NanoLab software package [19]. The fundamental theoretical framework underlying this method is described in detail in Refs. [20-22].

4. RESULTS AND DISCUSSION

Fig. 2a shows the *I-V* characteristics for three nanodevice configurations: G-MoS_2/WS_2-G, G-MoS_2/WS_2-Sil, and Sil-MoS_2/WS_2-G, over a bias voltage range from − 2 to + 2 V (G denotes graphene and Sil denotes silicene).

For the symmetric G-MoS_2/WS_2-G structure, the *I-V* characteristics exhibit a quasi-linear response over the entire investigated bias range from − 2 V to + 2 V, indicating relatively transparent contacts and a transport regime close to ohmic behavior (Fig. 2a, black curve). The current reaches values on the order of $1.8 \cdot 10^5$ nA at $|V| = 2$ V, corresponding to an effective differential conductance of approximately ~ $0.8 \cdot 10^5$ nS (~ 80 μS). The I-V curve displays weakly pronounced step-like features, visually reminiscent of current steps characteristic of the single-electron charging model of a nanocapacitor [23, 24]. At first glance, such behavior could be interpreted within the framework of single-electron transport, where electron transfer occurs via discrete charging events of the central region [25]. In this picture, charge accumulation on an "island" leads to Coulomb repulsion between nearby charges at the electrode–island interface, resulting in a temporary suppression of the current due to Coulomb blockade when the total charge prevents the addition or removal of an extra electron from the central part of the device [26, 27].

However, the geometrical parameters of the investigated structure render such an interpretation physically unlikely. The central MoS_2/WS_2 active region has extended dimensions (approximately 87 Å × 75 Å in the layer plane and a channel length of ~ 130 Å along the transport direction), which results in a large effective capacitance. An estimate of the capacitance within the parallel-plate capacitor approximation yields $C >> 10^{-18}$ F, so that the charging energy $E_C = e^2/2C$ is much smaller than the thermal energy $k_B T$, even at low simulation temperatures. Consequently, the condition $E_C >> k_B T$ required for the realization of Coulomb blockade and single-electron tunneling is not satisfied

in this system. Therefore, the observed weak nonlinearity of the *I-V* characteristics and the quasi-step-like features at high bias are not related to single-electron charging effects. Instead, they originate from the energy dependence of the density of states in the central MoS_2/WS_2 region, resonant interlayer tunneling, and contact effects at the graphene-MoS_2/WS_2 interface. Such behavior represents a characteristic manifestation of quantum-wave transport in an extended two-dimensional system and is fully consistent with the description provided by the NEGF formalism.

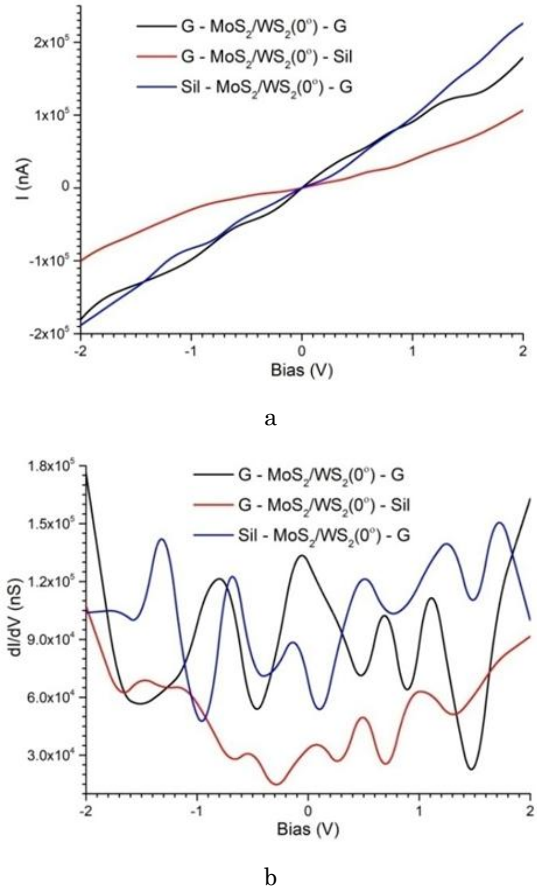

Fig. 2 – *I-V* characteristics (a) and differential conductance spectra (b) of MoS_2/WS_2 nanodevices with graphene and silicene electrodes at zero twist angle

In the case of the asymmetric G-MoS_2/WS_2-Sil configuration, a pronounced reduction of the current is observed compared to the symmetric graphene-based device (Fig. 2a, red curve). At the maximum bias of $|V| = 2$ V, the current reaches approximately ~ 10^5 nA, which is nearly 1.8 times lower than that of the G-MoS_2/WS_2-G structure. Accordingly, the effective differential conductance decreases to ~ $4 \cdot 10^4$ nS, whereas for the symmetric configuration it amounts to ~ $8 \cdot 10^4$ nS. The *I-V* characteristic of the asymmetric structure is marked by a substantially reduced slope and pro-nounced nonlinearity, particularly in the negative bias region. For instance, at − 1 V, the current in the G-MoS_2/WS_2-Sil configuration is only ~ $2.97 \cdot 10^4$ nA, while in the symmetric graphene device it exceeds ~ $9.8 \cdot 10^4$ nA.

The observed nonlinearity manifests itself in an asymmetric variation of the *I-V* slope upon bias polarity reversal and in the absence of quasi-linear behavior near zero bias. Such behavior indicates an increased effective contact resistance and less efficient matching of the density of states between the silicene electrode and the central MoS_2/WS_2 heterostructure. As a result, charge transport in this configuration becomes more sensitive to the interfacial electronic structure and is limited by barrier- and contact-induced effects, leading to current suppression and enhanced nonlinearity of the *I-V* characteristics compared to the symmetric graphene-based system.

For the inverted asymmetric Sil-MoS_2/WS_2-G structure, the current at positive bias voltages is the highest among all the investigated devices (Fig. 2a, blue curve). At 2 V, the current reaches approximately ~ $2.26 \cdot 10^5$ nA, which is about 1.3-1.4 times larger than that of the symmetric G-MoS_2/WS_2-G structure and more than twice the current observed in the G-MoS_2/WS_2-Sil configuration at the same bias. Accordingly, the effec-tive differential conductance at positive voltages at-tains ~ $1.1 \cdot 10^5$ nS, indicating the most transparent transport channel among the studied systems. The *I-V* characteristic of this structure exhibits the steepest slope for $V > 0$, whereas at negative voltages the current is significantly lower, reaching approximately − $1.9 \cdot 10^5$ nA at − 2 V, which highlights the pronounced asymmetry of the transport properties.

Such behavior points to a more efficient carrier injection from the silicene electrode under positive bias polarity. The observed current enhancement suggests the formation of contact-induced interfacial metallization at the silicene-MoS_2 interface, where the semimetallic nature of silicene interacts with the semiconducting MoS_2 layer, resulting in an effective nanosystem with metallic-like transport characteristics. This inter-pretation is consistent with the results reported by X. Li et al. [28], where Sil-MoS_2 superlattices were shown to exhibit novel band-structure features, including the emergence of multiple bands crossing the Fermi level, which is a direct signature of metallic behavior in the hybrid system. In addition, our earlier work [29] demonstrated that contact-induced metallization of the Sil-MoS_2 interface significantly enhances the transport characteristics of quasi-two-dimensional vdW nanodevices.

As in the case of the symmetric G-MoS_2/WS_2-G configuration, weakly pronounced quasi-step-like features are observed in the *I-V* characteristics of the Sil-MoS_2/WS_2-G structure, most prominently in the bias range $|V|$ 0.8-1.5 V. However, in contrast to single-electron devices, these features are not accompanied by current suppression and do not form plateaus, indicating their non-Coulombic origin. We attribute these quasi-steps to resonant interlayer tunneling, the energy dependence of the density of states, and contact effects at the electrode-MoS_2/WS_2 interface.

Thus, changing the electrode material leads not only to quantitative variations in the current magnitude but also to a qualitative reconstruction of the transport regime associated with the formation of interfacial metallic states. Overall, at $\theta = 0°$, the differences in the *I-V* characteristics of the three investigated nanodevices are predominantly governed by contact effects, while the contribution of moiré modulation is absent in this case.

The features observed in the *I-V* characteristics are directly reflected in the differential conductance spectra *dI*/*dV* (Fig. 2b). The *dI*/*dV* spectra calculated for the same nanodevice configurations over the bias range from – 2 V to 2 V exhibit a pronounced energy-dependent structure, which reflects the electronic density of states of the central MoS_2/WS_2 heterostructure as well as the decisive role of the electrode material.

For the symmetric G-MoS_2/WS_2-G structure, the differential conductance values lie in the range of $(6 \div 14)\cdot 10^4$ nS, and the *dI*/*dV* spectrum is characterized by an alternation of local maxima and minima. These features correlate with the weak nonlinearities observed in the *I-V* characteristics and originate from the energy dependence of the transmission coefficient, as well as from resonant tunneling through quasi-continuous electronic states of the MoS_2/WS_2 heterobilayer. The minima in *dI*/*dV* at certain bias voltages indicate the presence of pseudogaps associated with the band structure of the central region.

In the asymmetric G-MoS_2/WS_2-Sil configuration, the *dI*/*dV* spectra exhibit the lowest absolute values, on the order of $(2 \div 6)\cdot 10^4$ nS, as well as a pronounced asymmetry with respect to zero bias. In the low-bias and negative-bias regions, a substantial suppression of the differential conductance is observed, which is consistent with the reduced slope of the *I-V* characteristics and indicates the presence of an effective barrier at the graphene-MoS_2/WS_2-silicene interface. The smoothed character of the resonant features suggests less efficient hybridization between the electronic states of the electrodes and those of the central TMD heterostructure.

For the inverted asymmetric Sil-MoS_2/WS_2-G structure, the *dI*/*dV* spectra exhibit the largest amplitudes, reaching values of $(1.0 \div 1.6)\cdot 10^5$ nS at positive bias voltages. The spectra display pronounced resonant peaks whose density and amplitude increase significantly for $V > 0$, directly correlating with the maximum current observed in the *I-V* characteristics. These features indicate the formation of additional conducting channels near the Fermi level and represent the spectral signature of contact-induced interfacial metallization at the Sil-MoS_2 interface.

Thus, the analysis of the *dI*/*dV* spectra confirms that the observed nonlinearities and asymmetries in the *I-V* characteristics have a quantum-spectral origin and arise from the redistribution of the electronic density of states, resonant interlayer tunneling, and contact effects. In the absence of moiré modulation ($\theta = 0°$), the electrode material plays the dominant role in determining the shape of the *dI*/*dV* spectra and, consequently, the transport regime of the nanoheterostructure.

The analysis provides a baseline for the subsequent investigation of effects induced by finite moiré twist angles, where additional *dI*/*dV* peaks and enhanced nonlinear features in the *I-V* characteristics are expected.

Fig. 3 presents the *I-V* characteristics of three vdW nanodevice configurations – G-MoS_2/WS_2-G, G-MoS_2/WS_2-Sil, and Sil-MoS_2/WS_2-G – calculated for different twist angles between the MoS_2 and WS_2 layers ($\theta = 3°$, 6.2°, and 9.7°). The introduction of a moiré twist angle leads to a pronounced reconstruction of the transport characteristics compared to the $\theta = 0°$ case, reflecting the influence of the spatially modulated potential in the central region of the device.

For the symmetric device with graphene electrodes, the *I-V* characteristics retain a quasi-linear behavior over the entire bias range; however, a systematic variation of the curve slope is observed with increasing moiré twist angle. Upon introducing a small twist angle of $\theta = 3°$, the current at negative bias decreases to $\sim 1.5\cdot 10^5$ nA, corresponding to a reduction of approximately ~ 8 % compared to the untwisted structure. This decrease in conductance is associated with the formation of a long-period moiré superlattice, which induces partial localization of electronic states and reduces the effective transparency of the transport channel. With a further increase of the twist angle to $\theta = 6.2°$, the current rises to $\sim 1.7\cdot 10^5$ nA, while the effective conductance increases to $\sim 10^5$ nS. For $\theta = 9.7°$, the current reaches its maximum values of approximately $\sim 1.8\cdot 10^5$ nA at 2 V, corresponding to a 20 % enhancement in conductance relative to the $\theta = 3°$ regime. The increase in the slope of the *I-V* curves at larger twist angles indicates a weakening of moiré-induced localization and more efficient carrier tunnel-ing through the central MoS_2/WS_2 region. Thus, in the symmetric G-MoS_2/WS_2-G configuration, the moiré twist angle acts as an effective tuning parameter for the device conductance: small angles suppress the cur-rent due to state localization, whereas increasing the angle gradually drives the transport regime toward a more quasi-classical behavior with higher channel transparency.

For the structure with a graphene left electrode and a silicene right electrode (G-MoS_2/WS_2-Sil), the *I-V* characteristics exhibit pronounced nonlinearity and substantially lower absolute current values compared to the symmetric graphene-based device G-MoS_2/WS_2-G. At the maximum bias of 2 V, the current does not exceed $\sim 0.9\cdot 10^5$ nA, which is nearly 1.7-2 times smaller than in the symmetric configuration, where the current reaches $\sim 1.6\cdot 10^5$ nA. The strongest current suppression is observed at the small moiré twist angle $\theta = 3°$, particularly in the negative-bias region. For example, at – 2 V, the current amounts to approximately $\sim 10^5$ nA, whereas for the untwisted structure ($\theta = 0°$) and for larger twist angles ($\theta = 6.2°$ and 9.7°) it increases to $\sim 1.15\cdot 10^5$ nA.

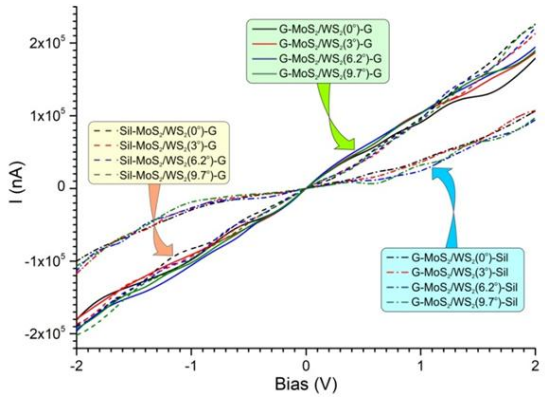

Fig. 3 – Effect of moiré twist angle on I-V characteristics of MoS_2/WS_2 nanodevices with graphene and silicene electrodes

With increasing twist angle to $\theta = 6.2°$ and 9.7°, a gradual increase in the current over the entire bias

range is observed, indicating a weakening of moiré-induced localization and a partial recovery of the transport channel transparency. Nevertheless, even at $\theta = 9.7°$, the slope of the *I-V* curves remains significantly smaller than that of the symmetric G-MoS_2/WS_2-G structure, and the effective differential conductance does not exceed ~ $5 \cdot 10^4$ nS, whereas it reaches ~ $8 \cdot 10^4$ nS for the symmetric graphene device. This behavior indicates that, even when moiré effects are weakened, the contact-induced mismatch of the density of states between graphene and silicene, as well as differences in their work functions, continue to play a dominant role in shaping the transport properties. As a result, transport in the G-MoS_2/WS_2-Sil structure remains limited by contact-induced effects, manifested in reduced current values and enhanced nonlinearity of the *I-V* characteristics compared to the symmetric configuration.

In the inverted asymmetric Sil-MoS_2/WS_2-G configuration, the influence of the moiré twist angle is most pronounced, manifesting itself both in the shape of the I-V characteristics and in the magnitude of the current. At a small twist angle of $\theta = 3°$, the *I-V* curve exhibits pronounced nonlinearity and reduced current values compared to larger twist angles. In particular, at 2 V the current amounts to approximately ~ $2 \cdot 10^5$ nA, while under negative bias ($V = -2$ V) it decreases to $I \approx 1.8 \cdot 10^5$ nA, indicating asymmetric carrier injection and an enhanced influence of long-period moiré modulation.

With an increase of the twist angle to $\theta = 6.2°$, the current rises over the entire bias range and the slope of the I-V characteristics becomes steeper, especially at positive biases. For example, at 2 V the current increases to ~ $2.15 \cdot 10^5$ nA, and the effective differential conductance reaches ~ $1.1 \cdot 10^5$ nS, reflecting a weakening of moiré-induced localization and an enhancement of the transport channel transparency. For the largest considered twist angle, $\theta = 9.7°$, the current attains its maximum values among all investigated angles. At 2 V, the current reaches ~ $2.25 \cdot 10^5$ nA, which is ~ 10 % higher than at $\theta = 3°$ and 5-8 % higher than at $\theta = 6.2°$. These findings indicate more efficient carrier transmission through the central MoS_2/WS_2 region and a substantial reduction in the influence of the moiré potential in the short-period modulation regime.

The asymmetry of the *I-V* characteristics with respect to zero bias persists for all twist angles and highlights the difference in carrier injection mechanisms from the silicene and graphene electrodes. In particular, under positive bias polarity, when silicene acts as the injecting electrode, a steeper *I-V* slope and enhanced conductance are observed, which is consistent with the formation of contact-induced metallic states at the Sil-MoS_2 interface.

Overall, as the moiré twist angle increases from 3° to 9.7°, all three types of nanodevices exhibit a clear tendency toward higher current values and a gradual approach of the *I-V* characteristics to a quasi-linear regime. This behavior indicates a progressive transition from transport governed by moiré-induced localization and miniband formation to a regime dominated by an effectively averaged interlayer potential. The differences among the three configurations highlight the crucial role of the electrode material: symmetric graphene contacts provide the most stable and predict-able transport behavior, whereas asymmetric structures involving silicene exhibit enhanced nonlinearity and a pronounced dependence of the *I-V* characteristics on bias polarity.

Fig. 4 presents the differential conductance spectra *dI*/*dV* for the G-MoS_2/WS_2-G, G-MoS_2/WS_2-Sil, and Sil-MoS_2/WS_2-G nanodevices at three values of the moiré twist angle. In contrast to the $\theta = 0°$ case, twisting the MoS_2 and WS_2 layers leads to the formation of a pronounced energy-dependent structure in the *dI*/*dV* spectra, reflecting the emergence of moiré-induced minibands and localized electronic states in the central region.

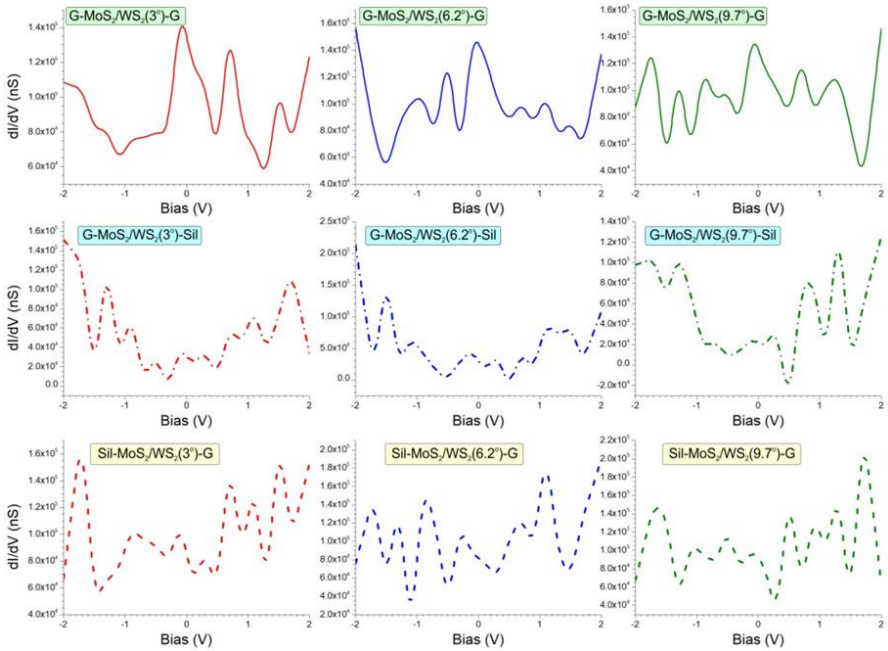

Fig. 4 – Twist-angle-dependent differential conductance spectra of MoS_2/WS_2 nanodevices with graphene and silicene electrodes

For the symmetric device with graphene electrodes, the dI/dV spectra exhibit well-defined oscillations across the entire bias-voltage range. At $\theta = 3°$, relatively broad and well-separated peaks are observed, corresponding to a long-period moiré superlattice and enhanced localization of electronic states. As the twist angle increases to 6.2°, the peaks become more numerous and shift in energy, indicating a reconstruction of the miniband structure. At $\theta = 9.7°$, the spectrum becomes smoother while retaining its oscillatory character, indicating the persistence of the moiré potential despite the reduction of its spatial period. Overall, the G-MoS_2/WS_2-G system exhibits a systematic evolution of the dI/dV spectra with increasing twist angle, reflecting a reconfiguration of the electronic structure of the central bilayer.

In the asymmetric configuration with a silicene right electrode, the absolute values of dI/dV are significantly lower than those of the symmetric graphene-based device, and the spectra are characterized by more pronounced nonlinearity. At $\theta = 3°$, a strong suppression of the conductance in the low-bias region is observed, accompanied by isolated resonant peaks, indicating the combined effect of moiré-induced localization and con-tact-induced mismatch of the density of states. At $\theta = 6.2°$, the spectrum becomes more structured; however, deep minima persist, pointing to the presence of pseudogaps in the effective transport spectral function. At $\theta = 9.7°$, dI/dV increases at larger $|V|$, indicating a weakening of localization and an enhancement of device transparency, although the asymmetry of the spectrum with respect to zero bias remains.

For the inverted asymmetric Sil-MoS_2/WS_2-G structure, the dI/dV spectra exhibit the highest oscillation amplitudes. Already at $\theta = 3°$, sharp peaks in the differential conductance are observed, which are associated with resonant tunneling through moiré-induced quasi-discrete states. At $\theta = 6.2°$, the peaks become more densely distributed and shift in energy, indicating an increasing complexity of the miniband structure. For $\theta = 9.7°$, the spectrum retains a high amplitude; however, the oscillations become less regular, reflecting the transition to a shorter-period moiré modulation and an enhanced role of contact effects. The asymmetry of dI/dV underscores the different carrier injection mechanisms from the silicene and graphene electrodes.

A comparative analysis of the dI/dV spectra shows that increasing the moiré twist angle from 3° to 9.7° leads to a gradual increase in the complexity of the energy-dependent structure of the differential conductance and to shifts of the resonant peaks. At small twist angles, localization effects and the formation of narrow minibands dominate, whereas at larger angles a more uniform energy distribution of electronic states is observed. The pronounced differences among the three configurations highlight the key role of the electrode material: graphene contacts yield more symmetric and regular spectra, while the presence of silicene enhances asymmetry and gives rise to more pronounced resonant features.

Thus, the dI/dV spectra confirm that both the moiré twist angle and the electrode type directly govern the spectral and transport properties of MoS_2/WS_2 heterostructures, providing a foundation for the design of tunable moiré nanoelectronic devices.

5. CONCLUSIONS

In this work, the electronic transport properties of vdW MoS_2/WS_2 nanoheterostructures with different electrode configurations (graphene and silicene) and moiré twist angles $\theta = 0°$, 3°, 6.2°, and 9.7° are investigated within the NEGF formalism. It is shown that at $\theta = 0°$, the shape of the I-V characteristics is governed primarily by contact effects, while the moiré modulation has no significant influence. Symmetric graphene contacts provide quasi-linear transport, whereas asymmetric configurations involving silicene exhibit reduced currents and pronounced nonlinearity. The introduction of a moiré twist angle leads to current suppression at small angles due to the localization of electronic states, and to an increase in current at larger angles as a result of the weakening of the moiré potential. For the Sil-MoS_2/WS_2-G configuration, maximum currents are observed under positive bias, which is interpreted as a manifestation of contact-induced interfacial metallization at the Sil-MoS_2 interface. The obtained results demonstrate the possibility of controlling the transport properties of MoS_2/WS_2 heterostructures through the moiré twist angle and the choice of electrode material, thereby opening prospects for the development of tunable nanoelectronic devices.

ACKNOWLEDGEMENTS

This work was supported by grant of the Ministry of Science and Higher Education of the Republic of Kazakhstan AP23488734.

REFERENCES

1. N. Shehzad, I. Iqbal, Y. Ahmad, M.-Q. Cai, *Int. J. Mod. Phys. B* **39**, 25501243 (2024) https://doi.org/10.1142/S0217979225501243.
2. C.-J. Kim, K.-H. Choi, Y. Lee, S. Kang, S. Yim, W. Song, J. Lim, S. Myung, S. S. Lee, S. Park, B.H. Hong, *Appl. Sci. Converg. Technol.* **34** No 2, 53 (2025) https://doi.org/10.5757/ASCT.2025.34.2.53.
3. G. Kipp, H.M. Bretscher, B. Schulte, D. Herrmann, K. Kusyak, M.W. Day, et al., *Nat. Phys.* **21**, 1926 (2025) https://doi.org/10.1038/s41567-025-03064-8.
4. X. Cheng, X. Fu, X. Li, W. Liao, J. Guo, L. Li, *Int. J. Mod. Phys. B* **38**, 2450074 (2024) https://doi.org/10.1142/S0217979224500747.
5. H. Xu, Y. Xue, Z. Liu, Q. Tang, T. Wang, X. Gao, Y. Qi, Y.P. Chen, C. Ma, Y. Jiang, *Small Sci.* **4**, 2300213 (2024) https://doi.org/10.1002/smsc.202300213.
6. J.-H. Baek, W. Choi, G.-H. Lee, *npj 2D Mater. Appl.* **9**, 823 (2025) https://doi.org/10.1038/s41699-025-00642-5.
7. Y. Wu, M. Sun, *Appl. Mater. Today* **37** No 14, 102101 (2024) https://doi.org/10.1016/j.apmt.2024.102101.
8. Q. Lin, H. Fang, A. Kalaboukhov, Y. Liu, Y. Zhang, M. Fischer, J. Li, J. Hagel, S. Brem, E. Malic, N. Stenger, Z. Sun, M. Wubs, S. Xiao, *Nat. Commun.* **15**, 8762 (2024) https://doi.org/10.1038/s41467-024-53083-x.

9. H. Wang, T.H. Ly, J. Zhao, *Newton* **1**, 100260 (2025) https://doi.org/10.1016/j.newton.2025.100260.
10. D. Sergeyev, A. Duisenova, A. Solovjov, N. Ismayilova, *Res. Phys.* **54**, 107140 (2023) https://doi.org/10.1016/j.rinp.2023.107140.
11. Y. Cao, V. Fatemi, S. Fang, K. Watanabe, T. Taniguchi, E. Kaxiras, P. Jarillo-Herrero, *Nature* **556**, 43 (2018) https://doi.org/10.1038/nature26160.
12. H. Yu, G.-B. Liu, W. Yao, *2D Mater.* **5**, 035021 (2018) https://doi.org/10.1088/2053-1583/aac065.
13. Z. Wang, D.A. Rhodes, K. Watanabe, T. Taniguchi, J.C. Hone, J. Shan, K.F. Mak, *Nature* **574**, 76 (2019) https://doi.org/10.1038/s41586-019-1591-7.
14. D.W. Latzke, W. Zhang, A. Suslu, T.-R. Chang, H. Lin, H.-T. Jeng, S. Tongay, J. Wu, A. Bansil, et al., *Phys. Rev. B* **91**, 235202 (2024) https://doi.org/10.1103/PhysRevB.91.235202.
15. J. Tang, S. Li, L. Zhan, S. Li, *Mater. Today Electron.* **11**, 100132 (2024) https://doi.org/10.1016/j.mtelec.2024.100132.
16. M. Yue, K. Zhang, M. Zhao, et al., *Nat. Commun.* **16**, 4018 (2025) https://doi.org/10.1038/s41467-025-59174-7.
17. J.P. Perdew, K. Burke, M. Ernzerhof, *Phys. Rev. Lett.* **77**, 3865 (1996) https://doi.org/10.1103/PhysRevLett.77.3865.
18. M. Kaur, R.S. Sawhney, D. Engles, J. Mol, *Graph. Model.* **71**, 184 (2017) https://doi.org/10.1016/j.jmgm.2016.10.017.
19. AtomistixToolKit with Virtual NanoLab ATK-VNL 2015.1. Available online: https://www.synopsys.com/ (accessed on 12 July 2022).
20. M. Brandbyge, J.L. Mozos, P. Ordejón, J. Taylor, K. Stokbro, *Phys. Rev. B* **65**, 165401 (2002) https://doi.org/10.1103/PhysRevB.65.165401.
21. B.G. Shohany, M.R. Roknabadi, A. Kompany, *Comput. Mater. Sci.* **144**, 280 (2018) https://doi.org/10.1016/j.commatsci.2017.12.031.
22. D. Sergeyev, N. Zhanturina, *Radioengineering* **28** No 4, 714 (2019) https://doi.org/10.13164/re.2019.0714.
23. J.R. J., J.T. Mazumder, A.B. Aloshious, R.K. Jha, *Nanoscale* **17**, 11960 (2025) https://doi.org/10.1039/D5NR00384A.
24. D. Sergeyev, N. Ashikov, N. Zhanturina, *Int. J. Nanosci.* **20** No 01, 2150007 (2021) https://doi.org/10.1142/S0219581X21500071.
25. P. Papadopoulou, K. Ovaliadis, E. Philippousi, M.P. Hanias, L. Magafas, S.G. Stavrinides, *Symmetry* **16**, 327 (2024) https://doi.org/10.3390/sym16030327.
26. A. Nasri, A. Boubaker, A. Kalboussi, *Discov. Electron.* **2**, 12 (2025) https://doi.org/10.1007/s44291-025-00053-2.
27. D. Sergeyev, *J. Nano- Electron. Phys.* **12** No 3, 03017 (2020) https://doi.org/10.21272/jnep.12(3).03017.
28. X. Li, S. Wu, S. Zhou, Z. Zhu, *Nanoscale Res. Lett.* **9**, 110 (2014) https://doi.org/10.1186/1556-276X-9-110.
29. D.M. Sergeyev, A.G. Duisenova, *Tech. Phys. Lett.* **47**, 417 (2021) https://doi.org/10.1134/S1063785021040295.

Електронний транспорт, керований кутом муару, у нанопристроях Ван-дер-Ваальса MoS_2/WS_2 з графеновими та силіценовими електродами

D. Sergeyev[1,2], E. Yeskibayev[2]

[1] *K. Zhubanov Aktobe Regional University, 030000 Aktobe, Kazakhstan*
[2] *T. Begeldinov Aktobe Avation Institute, 030012 Aktobe, Kazakhstan*

Представлено теоретичне дослідження електронного транспорту у Ван-дер-Ваальсових нанопристроях на основі гетеробішарів MoS_2/WS_2 з різними конфігураціями електродів, включаючи контакти на основі графену та силіцену. Вплив відносного скручування між шарами MoS_2 та WS_2 систематично аналізується для кутів скручування $\theta = 0°$, 3°, 6,2° та 9,7°, що відповідають різним режимам модуляції муарової надґратки. Квантові транспортні розрахунки виконуються в рамках формалізму нерівноважних функцій Гріна, що дозволяє послідовно описувати контактні ефекти та залежні від напруги характеристики передачі. Показано, що за відсутності скручування транспортні властивості переважно визначаються матеріалом електрода. Введення малого кута скручування призводить до придушення струму через локалізацію електронних станів, викликаних муаровим ефектом, тоді як більші кути скручування призводять до підвищеної провідності. Інвертована конфігурація силіцен–MoS_2/WS_2–графен демонструє найвищий струм, що пояснюється металізацією інтерфейсу, що виникає внаслідок контакту силіцен-MoS_2. Ці результати демонструють, що як кут повороту, так і матеріал електрода забезпечують ефективні засоби для налаштування транспортних властивостей наноелектронних пристроїв на основі MoS_2/WS_2.

Ключові слова: Нанопристрої Ван-дер-Ваальса MoS_2/WS_2, Муарові гетероструктури TMD, Квантовий транспорт, Контактно-індуковані ефекти, Нерівноважна функція Гріна.